LETTERS IN BIOMATHEMATICS
An International Journal

RESEARCH ARTICLE

OPEN ACCESS

Effects of a Generalised Anti-CD147 Drug on Tumor Angiogenesis - A Pharmacological Model

Bhooma Sreedaran[1], Vimala Ponnuswamy[1]

[1] Department of Mathematics, Anna University, Chennai, India

ABSTRACT

Tumor angiogenesis is a process of growing new blood vessels from existing ones. The process of inhibiting tumor angiogenesis is anti-angiogenesis. There is a high incidence of Cluster of Differentiation 147 (CD147) on tumor surfaces and this is an important contributing factor to drive tumor angiogenesis. In this paper, mathematical models of anti-angiogenesis are presented which inculcates injecting a generalized anti-CD147 drug into the tumor tissue. Equations relating to the concentrations of Endothelial Cells (ECs), Tumor Angiogenesis Factors (TAFs), Fibronectin, Matrix Metallo Proteinases (MMPs), CD147, anti-CD147 drug and tumor cells are modeled as Partial Differential Equations (PDEs). The drug-receptor binding kinetics are considered in the model. Different drug dose options are also examined. The effect of the drug on EC migration are presented. The simulations are performed using COMSOL Multiphysics 5.4 software and a particular anti-CD147 drug is used for the simulations. The results indicate that the anti-CD147 drug considered in the simulations, help in slowing down the angiogenesis process with sufficient drug dose conditions as expected. Under specific conditions, these results agree well with the existing theoretical and experimental results. Further, it is seen that the application of the drug on EC migration effectively curbs the angiogenesis process.

ARTICLE HISTORY
Received June 22, 2023
Accepted December 27, 2023

KEYWORDS
Mathematical Modeling, TAFs, MMPs, Anti-CD147 Drug, Drug Dose

1. Introduction

Angiogenesis is the process of growing new blood vessels from already existing vessels. Tumor angiogenesis is a crucial process for the survival of the tumor. In 1971, Folkman proposed that tumors do not have the capacity to sustain with only diffusion of nutrients from their surrounding tissues and they require their own supply of blood vessels to grow beyond 1mm - 2mm in diameter (Folkman, 1971). At this juncture, tumor angiogenesis is initiated by the tumor and this is done by secreting Tumor Angiogenesis Factors (TAFs). Among TAFs, Vascular Endothelial Growth Factor (VEGF) plays the most important role in angiogenesis. These TAFs diffuse into the surroundings and create a chemical gradient. The Endothelial Cells (ECs) move in response to this gradient resulting in chemotaxis. The ECs move towards the tumor and tube formation occurs. Branching (sprout formation) then occurs along with loop formation or anastomosis (Paweletz & Knierim, 1989). There are other factors which help in angiogenesis like fibronectin which is an adhesion molecule and it creates a gradient. The movement of the ECs towards this bound substance is termed haptotaxis. The ECs will bind to this bound fibronectin and hence move slowly towards the tumor (Paweletz & Knierim, 1989). Matrix Metallo Proteinases (MMPs) fall under a class of enzymes which help in degrading the Extra Cellular Matrix (ECM) and ensuring a space for the tumor to grow new blood vessels. The different roles of MMPs in angiogenesis are reviewed by Rundhaug (Rundhaug, 2005). MMPs are largely induced by Cluster of Differentiation147 (CD147) or Extracellular Matrix Metallo Proteinases Inducer (EMMPRIN). CD147 is a transmembrane glycoprotein which is found in large quantities on tumor surfaces. Its major role is in inducing MMPs and increasing the concentration of VEGF by activating the Vascular Endothelial Growth Factor Receptor-2 (VEGFR-2) (Wang et al., 2016). When the tumor becomes vascularized, it renders the escape of many cells and these cells move through the blood stream to set up secondary tumors elsewhere in the body. This process of spreading of the tumor is termed as metastasis (Leber & Efferth, 2009). In 1972, Folkman also proposed that anti-angiogenic therapy, a process of inhibiting angiogenesis, might prove to be an essential treatment strategy to prevent metastasis (Folkman, 1972). There are other factors that are secreted by the tumor like endostatin and angiostatin, which are termed as anti-angiogenic factors. The inhibition of angiogenesis depends on the concentrations of endostatin and

CONTACT Bhooma Sreedaran mathsbhooma@gmail.com

angiostatin (Lupo et al., 2017). Inhibition/down-regulation of CD147 resulted in reduction of VEGF concentration leading to slower growth of the tumor as seen experimentally in Chen et al. (Chen et al., 2012). Inhibition of CD147 is done by using anti-CD147 antibody (Wang et al., 2012) or the down-regulation of CD147 is done by using RNAi (Chen et al., 2015). Mathematically modeling the growth of tumor angiogenesis and the process of inhibition, help us in under- standing the details of experimental design. Modeling the aspects of avascular tumor growth in tumor spheroids started in the 1980s. However, a more realistic approach was developed in 1998 by Anderson and Chaplain (Anderson & Chaplain, 1998), in which they described a capillary sprout formation using continuous and discrete mathematical models. Mathematical models of anti-angiogenesis were developed in the 1990s but were brought to a fine shape by Anderson et al. (Anderson et al., 2000). In their model, the authors considered the concentration of angiostatin and its effects on the ECs. They discussed the suppression of the secondary tumor by the primary tumor and also considered the size of the tumor. They concluded that larger the size of the primary tumor, more will be the inhibition on angiogenesis. Zhao et al. (Zhao et al., 2017), extended the work of Anderson et al. and developed a three-dimensional model for angiogenesis and included the effects of angiostatin (derived from primary tumor) on angiogenesis (Anderson et al., 2000). They concluded that angiostatin has the potential to inhibit tumor vascular growth, branching and anastomosis. Modeling in anti-angiogenic therapy has seen many advances in the past decades, specifically pharmacological modeling of drug discovery and drug delivery. The crux of a pharmacological model is to study a biological system under the impact of a drug. Further, the amount of the drug to be given and the duration the drug has to be administered are determined with the help of a pharmacological model. This has a greater reach in assisting the course of therapy for individual patients (Krzyzanski, 2013). The kinetics of the drug and receptor help in exploring the correlation between the drug concentration and the drug impact. The binding of a drug to a receptor result in elucidating the response of a drug (Dick, 2011). This interaction leads to the formation of a drug-receptor complex. The development of a drug-receptor complex reveals the amount of receptor molecules engaged by the drug molecules. This is measured by the affinity of the drug to the receptor. Affinity for a drug is defined as the attraction of the drug to the receptor and the time for which the binding sustains. The reverse measure is dissociation, that is, the detachment of the drug-receptor complex into drug and receptor. In general, if D represents the drug concentration and R represents the receptor concentration, then DR represents the drug-receptor complex concentration and $D + R \underset{k_{-1}}{\overset{k_{+1}}{\rightleftarrows}} DR$ represents the equation for the complex. Here, k_{+1} and k_{-1} are the association and dissociation constants, respectively. The binding kinetics are largely expressed with the help of equilibrium dissociation constant which is defined as $K_D = \frac{k_{-1}}{k_{+1}}$.

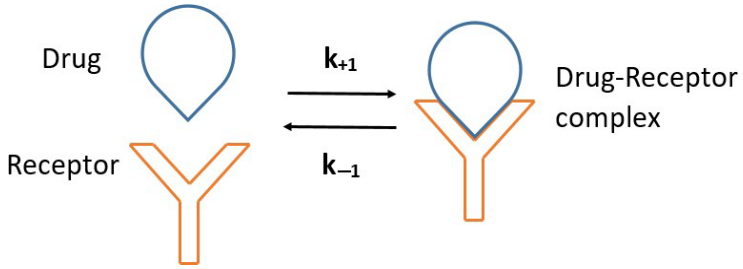

Figure 1: The Drug-Receptor Binding

Figure 1 illustrates the binding of the drug to the receptor resulting in the formation of the complex and the process of dissociation of the complex into drug and receptor. The response produced due to the binding of the drug to the receptor, can either be activation of the receptor or blockage of the receptor action. The former is termed as an agonist and the latter as an antagonist. Among antagonists, competitive antagonists are the main focus for various therapies. A competitive antagonist is one which competes with the agonists to occupy the same sites of the receptor, thus resulting in obstruction of the agonist. The response of the drug is mathematically expressed by the $E_{\max}$ model. The $E_{\max}$ model for agonists is given by $E = E_{\max}\frac{C}{C+K_D}$, where C is the agonist concentration, E is the effect produced, $E_{\max}$ is the maximum effect produced by the agonist and K_D is the equilibrium dissociation constant of the agonist. The $E_{\max}$ model for competitive antagonists is given by $E = E_{\max}\frac{C}{C+K_D\left(1+\frac{D}{K_{D,a}}\right)}$, where $C, E, E_{\max}$ and K_D are the quantities for agonist as before, D is the antagonist concentration and $K_{D,a}$ is the equilibrium dissociation constant of the antagonist (Salhabdeen & Niahsitha, 2017). In a paper by Billy et al., the authors developed a mathematical formulation using the classical $E_{\max}$ model for angiostatin therapy (Billy et al., 2009). They found that there is a critical drug threshold and if the treatment duration is increased beyond this threshold, the treatment leads to a loss in drug efficacy. In Liao et al., the dosages of a drug were considered and an expression for the rate of the dosage was modeled as a function of time (Liao et al., 2014), indicating intermittent

drug dosages.

Also, the efficacy of the drug was considered by comparing continuous dosing and intermittent dosing. Cai et al. developed a multi-scale model to study the effects of endostatin drug on tumor angiogenesis (Cai et al., 2016). Having considered drug injection rate at different times, they concluded that large doses of the drug causes EC apoptosis and reduction in the size of the tumor at the 'emergence of angiogenic phase'. In a paper by Oduola and Li, a model for tumor drug effects using stochastic hybrid system was developed (Oduola & Li, 2018). A multiscale model was developed for the subcellular, cellular and multicellular levels. They showed that there was a repression of tumor growth when the drug dosage was high. In the present paper, generalized mathematical models are developed to study the inhibition of TAFs and MMPs that are induced by CD147. This is done with the help of a generalized anti-CD147 drug. The motivation of this research is the fact that CD147 acts as a major driving force for tumor angiogenesis to take place. An anti-CD147 antibody can block the increase in the concentrations of TAFs and MMPs that are induced by CD147 (Wang et al., 2016). The main goals of these models are to understand the effect of anti-CD147 drug and to determine a possible drug dosage regimen. The models are developed with the pharmacological effects of the drug taken into account. The effect of the drug is considered with the help of the $E_{\max}$ model for competitive antagonists. The drug-receptor binding kinetics are used for the drug binding to the CD147 receptor which is present on tumor cells. The novelty of the models is that it considers a general anti-CD147 drug concentration and the effect of the drug on TAFS and MMPs. The tumor cell proliferation is also inhibited with the help of the drug. The drug dose conditions and the effect of the drug directly applied to EC migration are also examined. The injection rate of the drug is taken into account by considering a temporal function that releases the drug after a certain period of time.

2. Mathematical Model

This paper deals with generalized pharmacological-based mathematical models of anti-CD147 drug and its effects on ECs, TAFs, MMPs and tumor proliferation under different drug doses. The notations for the dimensional quantities are as follows- n^* for density of ECs, c^* for concentration of TAFs, f^* for concentration of fibronectin, m^* for concentration of MMPs, b^* for concentration of CD147, d^* for concentration of antiCD147 drug and T^* for density of tumor cells. The corresponding non-dimensional quantities are denoted by n, c, f, m, b, d and T, respectively. To examine the effect of the anti-CD147 drug on EC migration, two cases are considered - in the absence of the drug on EC chemotaxis and in the presence of the drug on EC chemotaxis.

2.1 Case 1: In the absence of the drug on EC chemotaxis

The CD147 effect is assumed to be implicit on ECs, through TAFs, fibronectin and MMPs. The ECs react to TAFs in a chemotactic manner. Also, the haptotaxis term for fibronectin and the random motility of the ECs are considered. Since the anti-CD147 drug targets CD147, its effect on ECs is not explicitly considered. Thus, the EC conservation equation is given by

$$\frac{\partial n^*}{\partial t^*} = D_n^* \nabla^2 n^* - \nabla \cdot (\chi c^* n^* \nabla c^*) - \nabla \cdot (\rho_0^* n^* \nabla f^*) \qquad (1)$$

where D_n^* is the co-efficient of diffusion of ECs, $\chi(c^*)$ is the TAF chemotaxis function which is given by $\chi(c^*) = \frac{(\chi_0^* k^*)}{(k^* + c^*)}$, with $\chi_0^* > 0$ as the co-efficient of TAF chemotaxis, $k^* > 0, \rho_0^* > 0$ is the co-efficient of fibronectin haptotaxis and t^* is the dimensional time. Experimental evidence suggests that CD147 increases VEGF concentration (Wang et al., 2016) and since the drug is being injected to make CD147 inactive, there is inhibition of TAF production by CD147. Pharmacological modeling is used to consider the effect of the drug, with the help of the Emax model. The production of TAFs by tumor cells is also considered. Thus, the equation for the concentration of TAFs is taken to be

$$\frac{\partial c^*}{\partial t^*} = -\eta^* n^* c^* + \left[\frac{E_{\max_{b,c}}}{1 + \frac{K_{D_{b,c}}^*}{b^*}\left(1 + \frac{d^*}{K_{D_{d,c}}^*}\right)} \right] b^* + \lambda_1^* T^* \qquad (2)$$

where η^* is the consumption rate of TAF by the ECs, $E_{\max_{b,c}}$ is the maximum effect of CD147 on TAFs, λ_1^* is the rate of production of TAFs by tumor cells, $K_{D_{b,c}}^*$ and $K_{D_{d,c}}^*$ are the equilibrium dissociation constants of CD147 and anti-CD147 drug, respectively, both with respect to TAF. The fibronectin is produced by ECs and is also taken up by the ECs. The effect of MMPs on fibronectin are considered in the equation. Hence, the fibronectin concentration equation is given as

$$\frac{\partial f^*}{\partial t^*} = \beta^* n^* - \gamma^* n^* f^* - \kappa^* m^* f^* \qquad (3)$$

where β^* is the rate of production of fibronectin by the ECs, γ^* is the rate of consumption of fibronectin by ECs, κ^* is the uptake rate of fibronectin by MMPs. The concentration of MMPs is increased by CD147 (Wang et al., 2016) and this is inhibited with the help of the drug using the $E_{\max}$ model. The diffusion and decay of the MMPs are also considered. The production of MMPs by tumor cells are included. Hence, the MMP equation is given by

$$\frac{\partial m^*}{\partial t^*} = D_m^* \nabla^2 m^* - \sigma^* m^* + \left[\frac{E_{\max\, b,m}}{1 + \frac{K^*_{D_{b,m}}}{b^*}\left(1 + \frac{d^*}{K^*_{D_{d,m}}}\right)}\right] b^* + \lambda_2^* T^* \qquad (4)$$

where D_m^* is the diffusion co-efficient of the MMPs, σ^* is the decay rate of the MMPs, $E_{\max\, b,m}$ is the maximum effect of CD147 on MMPs, λ_2^* is the rate of production of MMPs by tumor cells, $K^*_{D_{b,m}}$ and $K^*_{D_{d,m}}$ are the equilibrium dissociation constants of CD147 and anti-CD147 drug, respectively, both with respect to MMPs. The CD147 conservation equation consists of the diffusion of CD147, natural decay of CD147 and the binding effect. The drug binds to the CD147 receptor present on tumor cells which is considered through the binding term. Therefore, the equation for CD147 is given by

$$\frac{\partial b^*}{\partial t^*} = D_b^* \nabla^2 b^* - \delta^* b^* - \left[\frac{B_{\max_b}}{1 + \frac{K^*_{D_{b,b}}}{b^*}\left(1 + \frac{d^*}{K^*_{D_{d,b}}}\right)}\right] T^* \qquad (5)$$

where D_b^* is the diffusion co-efficient of CD147, δ^* is the decay rate of CD147, $B_{\max\, b}$ is the maximum binding, $K^*_{D_{b,b}}$ and $K^*_{D_{d,b}}$ are the equilibrium dissociation constants of CD147 and anti-CD147 drug, respectively, both with respect to CD147. The CD147 molecules that are shed by extracellular vesicles (Hatanaka et al., 2019), also bind to the CD147 receptor in a homophilic manner (Hanna et al., 2003) and hence the term $K^*_{D_{b,b}}$ is considered. The anti-CD147 drug will diffuse into the cells and will have a natural decay. The rate of injection is considered as a function of time. The binding of the drug to the CD147 receptor is considered as a binding term. Hence, the equation for the anti-CD147 drug is given by

$$\frac{\partial d^*}{\partial t^*} = D_d^* \nabla^2 d^* - \omega^* d^* + a(t^*) - \left[\frac{B_{max_d}}{1 + \frac{K^*_{D_{d,b}}}{d^*}\left(1 + \frac{b^*}{K^*_{D_{b,d}}}\right)}\right] T^* \qquad (6)$$

where D_d^* is the diffusion co-efficient of anti-CD147 drug, ω^* is the decay rate of anti-CD147 drug, $B_{\max}$ is the maximum binding, $K^*_{D_{d,b}}$ and $K^*_{D_{b,d}}$ are the equilibrium dissociation constants of anti-CD147 drug and CD147, respectively, both with respect to CD147, $a(t^*)$ is the injection rate of the drug given by $a(t^*) = (t^* - t_i^*)^{p^*} e^{-(t^* - t_i^*)\omega^*}$, where $p^* = t^*\omega^*$. The function $a(t^*)$ ensures that the maximum drug released is after a certain time $t^* > t_i^*$. This is helpful when considering a drug delivery vehicle where the drug is not immediately released (Phipps, 2009). The tumor cells proliferate and this is inhibited/suppressed with the help of the drug. There is also death of tumor cells due to apoptosis and necrosis. The diffusion of tumor cells is also considered. Hence, the equation for tumor cell density is given by

$$\frac{\partial T^*}{\partial t^*} = D_T^* \nabla^2 T^* - \alpha_1^* T^* - \alpha_2^* T^* + \mu^* T^* (1 - b^*)\left(1 - \frac{T^*}{T_0^*}\right)\left[\frac{E_{\max_{b,T}}}{1 + \frac{K^*_{D_{b,b}}}{b^*}\left(1 + \frac{d^*}{K^*_{D_{d,b}}}\right)}\right] \qquad (7)$$

where D_T^* is the diffusion co-efficient of tumor cells, α_1^* is the necrosis rate, α_2^* is the apoptosis rate, μ^* is the CD147 on tumor cells, $K^*_{D_{b,b}}$ and $K^*_{D_{d,b}}$ are the equilibrium dissociation constants of CD147 and anti-CD147 drug, respectively, both with respect to CD147. The above equations Eq. 1 - Eq. 7, are assumed to hold in a domain of square length L with $x = 0$ representing the parent blood vessel and $x = L$ representing the tumor, while $y = 0$ and $y = L$ represent the surrounding tissue. No-flux boundary conditions are assumed on the boundaries of the square. The boundary conditions are therefore given by

$$\begin{cases} \hat{n}\cdot(-D_n^*\nabla n^* + \chi(c^*)n^*\nabla c^* + \rho_0^* n^*\nabla f^*) & = 0 \\ \hat{p}\cdot(-D_m^*\nabla m^*) & = 0 \\ \hat{q}\cdot(-D_b^*\nabla b^*) & = 0 \\ \hat{r}\cdot(-D_d^*\nabla d^*) & = 0 \\ \hat{s}\cdot(-D_T^*\nabla T^*) & = 0. \end{cases} \tag{8}$$

where $\hat{n}, \hat{p}, \hat{q}, \hat{r}$ and $\hat{s}$ are the appropriate unit normal vectors on the square boundaries.

2.2 Case 2: In the presence of the drug on EC chemotaxis

The ECs move faster due to the dominating chemotaxis effect which is increased by CD147. Thus, the drug is directly applied to EC chemotaxis through the $E_{\max}$ term. The ECs migrate in response to chemotaxis due to TAFs and haptotaxis due to fibronectin. The random motility of the ECs is also considered. Hence, the EC conservation equation is given by

$$\frac{\partial n^*}{\partial t^*} = D_n^*\nabla^2 n^* - \nabla\cdot\left[\chi(c^*)\frac{E_{\max_c}}{1+\frac{K_{D_{b,c}}^{b^*}}{b^*}\left(1+\frac{d^*}{K_{D_{d,c}}^*}\right)}n^*\nabla c^*\right] - \nabla\cdot(\rho_0^* n^*\nabla f^*) \tag{9}$$

where $E_{\max_c}$ is the maximum effect of CD147 on chemotaxis and $K_{D_{b,c}}^*$ and $K_{D_{d,c}}^*$ are respectively the equilibrium dissociation constants of CD147 and anti-CD147 drug both with respect to TAF.The equations for the concentration of TAFs, fibronectin, MMPs, CD147, anti-CD147 drug and tumor cell density is taken as in Case 1. The equation 9 along with equations $2-7$ are assumed to hold in a square of length L as in Case 1. No-flux boundary conditions are assumed on the boundaries of the square and therefore, the boundary conditions are given by

$$\begin{cases} \hat{n}.\left(-D_n^*\nabla n^* + \left[\chi(c^*)\frac{E_{\max c}}{1+\frac{K_{D_{b,c}}^*}{b^*}\left(1+\frac{d^*}{K_{D_{d,c}}^*}\right)}n^*\nabla c^*\right] + \rho_0^* n^*\nabla f^*\right) & = 0 \\ \hat{p}\cdot(-D_m{}^*\nabla m^*) & = 0 \\ \hat{q}\cdot(-D_b{}^*\nabla b^*) & = 0 \\ \hat{r}\cdot(-D_d{}^*\nabla d^*) & = 0 \\ \hat{s}.(-D_T{}^*\nabla T^*) & = 0. \end{cases} \tag{10}$$

where $\hat{n}, \hat{p}, \hat{q}, \hat{r}$ and $\hat{s}$ are the appropriate unit normal vectors on the square boundaries.

2.3 Non-dimensionalization

Non-dimensionalization of equations 1 - 7 with boundary conditions from 8 for Case 1 and equation 9 along with equations $2-7$ with boundary conditions from equation 10 for Case 2, is accomplished with the help of appropriate variables given by $n=\frac{n^*}{n_0}, c=\frac{c^*}{c_0}, f=\frac{f^*}{f_0}, m=\frac{m^*}{m_0}, b=\frac{b^*}{b_0}, d=\frac{d^*}{d_0}, T=\frac{T^*}{T_0}, t=\frac{t^*}{\tau}$. Therefore, the non-dimensional equations for Case 1 are given by

$$\begin{cases} \frac{\partial n}{\partial t} & = D\nabla^2 n - \nabla.\left(\frac{\chi}{1+\alpha c}n\nabla c\right) - \nabla.(\rho n\nabla f) \\ \frac{\partial c}{\partial t} & = -\eta nc + \left[\frac{E_{max_{b,c}}}{1+\frac{K_{D_{b,c}}}{b}\left(1+\frac{d}{K_{D_{d,c}}}\right)}\right]b + \lambda_1 T \\ \frac{\partial f}{\partial t} & = \beta n - \gamma nf - \kappa mf \\ \frac{\partial m}{\partial t} & = D_m\nabla^2 m - \sigma m + \left[\frac{E_{max_{b,m}}}{1+\frac{K_{D_{b,m}}}{b}\left(1+\frac{d}{K_{D_{d,m}}}\right)}\right]b + \lambda_2 T \\ \frac{\partial b}{\partial t} & = D_b\nabla^2 b - \delta b - \left[\frac{B_{max_b}}{1+\frac{K_{D_{b,b}}}{b}\left(1+\frac{d}{K_{D_{d,b}}}\right)}\right]T \\ \frac{\partial d}{\partial t} & = D_d\nabla^2 d - \omega d + a(t) - \left[\frac{B_{max_d}}{1+\frac{K_{D_{d,b}}}{d}\left(1+\frac{b}{K_{D_{b,d}}}\right)}\right]T \\ \frac{\partial T}{\partial t} & = D_T\nabla^2 T - \alpha_1 T - \alpha_2 T + \mu T(1-b)\left(1-\frac{T}{T^*}\right)\left[\frac{E_{max_{b,T}}}{1+\frac{K_{D_{b,b}}}{b}\left(1+\frac{d}{K_{D_{d,b}}}\right)}\right]. \end{cases} \tag{11}$$

where $a(t) = (t - t_i)^p \exp^{-(t-t_i)\omega}$ and $p = t\omega$ with boundary conditions

$$\begin{cases} \hat{n} \cdot \left(-D\nabla n + \frac{\chi}{1+\alpha c} n\nabla c + \rho n \nabla f\right) & = 0 \\ \hat{p} \cdot (-D_m \nabla m) & = 0 \\ \hat{q} \cdot (-D_b \nabla b) & = 0 \\ \hat{r} \cdot (-D_d \nabla d) & = 0 \\ \hat{s} \cdot (-D_T \nabla T) & = 0. \end{cases} \tag{12}$$

$$\begin{cases} \frac{\partial n}{\partial t} & = D\nabla^2 n - \left[\nabla . \left(\frac{\chi}{1+\alpha c} \frac{E_{max_c}}{1+\frac{K_{D_{b,c}}}{b}\left(1+\frac{d}{K_{D_{d,c}}}\right)} n\nabla c\right)\right] - \nabla . \left(\rho n \nabla f\right) \\ \frac{\partial c}{\partial t} & = -\eta n c + \left[\frac{E_{max_{b,c}}}{1+\frac{K_{D_{b,c}}}{b}\left(1+\frac{d}{K_{D_{d,c}}}\right)}\right] b + \lambda_1 T \\ \frac{\partial f}{\partial t} & = \beta n - \gamma n f - \kappa m f \\ \frac{\partial m}{\partial t} & = D_m \nabla^2 m - \sigma m + \left[\frac{E_{max_{b,m}}}{1+\frac{K_{D_{b,m}}}{b}\left(1+\frac{d}{K_{D_{d,m}}}\right)}\right] b + \lambda_2 T \\ \frac{\partial b}{\partial t} & = D_b \nabla^2 b - \delta b - \left[\frac{B_{max_b}}{1+\frac{K_{D_{b,b}}}{b}\left(1+\frac{d}{K_{D_{d,b}}}\right)}\right] T \\ \frac{\partial d}{\partial t} & = D_d \nabla^2 d - \omega d + a\,(t) - \left[\frac{B_{max_d}}{1+\frac{K_{D_{d,b}}}{d}\left(1+\frac{b}{K_{D_{b,d}}}\right)}\right] T \\ \frac{\partial T}{\partial t} & = D_T \nabla^2 T - \alpha_1 T - \alpha_2 T + \mu T\,(1-b)\left(1-\frac{T}{T^*}\right)\left[\frac{E_{max_{b,T}}}{1+\frac{K_{D_{b,b}}}{b}\left(1+\frac{d}{K_{D_{d,b}}}\right)}\right]. \end{cases} \tag{13}$$

where $a(t) = (t - t_i)^p \exp^{-(t-t_i)\omega}$ and $p = t\omega$ and the boundary conditions are given by

$$\begin{cases} \hat{n} \cdot \left(-D\nabla n + \left[\frac{\chi}{1+\alpha c} \frac{E_{\max\, c}}{1+\frac{K_{D_{b,c}}}{b}\left(1+\frac{d}{K_{D_{d,c}}}\right)} n\nabla c\right] + \rho n \nabla f\right) & = 0 \\ \hat{p} \cdot (-D_m \nabla m) & = 0 \\ \hat{q} \cdot (-D_b \nabla b) & = 0 \\ \hat{r} \cdot (-D_d \nabla d) & = 0 \\ \hat{s} \cdot (-D_T \nabla T) & = 0. \end{cases} \tag{14}$$

where the non-dimensional quantities in both cases are given by

$$D = \frac{D_n^* \tau}{L^2}, \chi = \frac{\chi_0^* c_0 \tau}{L^2}, \alpha = \frac{c_0}{k^*}, \rho = \frac{\rho_0^* f_0 \tau}{L^2}, \eta = \eta^* n_0 \tau, \lambda_1 = \lambda_1^* \tau \frac{T_0}{c_0}, \beta = \frac{\beta^* n_0 \tau}{f_0}, \gamma = \gamma^* n_0 \tau, \kappa = \kappa^* m_0 \tau$$

$$D_m = \frac{D_m{}^* \tau}{L^2}, \sigma = \sigma^* \tau, \lambda_2 = \lambda_2^* \tau \frac{T_0}{m_0}, D_b = \frac{D_b{}^* \tau}{L^2}, \delta = \delta^* \tau, D_d = \frac{D_d{}^* \tau}{L^2}, \omega = \omega^* \tau, at = \frac{at^*}{\tau}, D_T = \frac{D_{T^*} \tau}{L^2}$$

$$\alpha_1 = \alpha_1^* \tau, \alpha_2 = \alpha_2^* \tau, \mu = \mu^* \tau, T^* = \frac{T_0^*}{T_0}, K_{D_{b,c}} = \frac{K_{D_{b,c}}^*}{R_c}, K_{D_{d,c}} = \frac{K_{D_{d,c}}^*}{R_d}, K_{D_{b,m}} = \frac{K_{D_{b,m}}^*}{R_m}, K_{D_{d,m}} = \frac{K_{D_{d,m}}^*}{R_d}$$

$$K_{D_{b,b}} = \frac{K_{D_{b,b}}^*}{R_b}, K_{D_{d,b}} = \frac{K_{D_{d,b}}^*}{R_d}$$

where R_c, R_m, R_b and R_d are the receptor concentrations of TAFs, MMPs, CD147 and anti-CD147 drug, respectively, with $L = 2$ mm and $\tau = 1.5$ days (Anderson & Chaplain, 1998), $n_0 = 2.5 \times 10^6 \text{cellcm}^{-3}$ (Liao et al., 2014), $c_0 \approx f_0 \approx 10^{-10} M$ (Anderson & Chaplain, 1998), $m_0 = 500 \text{ngml}^{-1}$ (Wróbel-Roztropiński et al., 2021), $b_0 = 20 \text{ngml}^{-1}$ (Amit-Cohen et al., 2013), $R_c = 1nM$ (Li et al., 2002), $R_m = 0.9688\mu M$ (Wu et al., 2013), $R_b = 138\mu M$ (Hanna et al., 2003) and $R_d = 50nM$ [present work]. The initial conditions in both cases are taken to be

$$\begin{cases} n(x,y,0) = e^{-\frac{x^2}{\varepsilon}}\sin^2(6\pi y), & c(x,y,0) = k_1 e^{-\frac{(1-x)^2}{\varepsilon_1}}, \\ f(x,y,0) = k_2 e^{-\frac{x^2}{\varepsilon_2}}, & m(x,y,0) = k_3 e^{-\frac{(1-x)^2}{\varepsilon_3}}, \\ b(x,y,0) = k_4 e^{-\frac{(1-x)^2}{\varepsilon_4}}, & d(x,y,0) = k_5 e^{-\frac{(1-x)^2}{\varepsilon_5}} \\ T(x,y,0) = k_6 e^{-\frac{x^2}{\varepsilon_6}}, & (x,y) \in [0,1] \times [0,1] \end{cases} \quad (15)$$

where $\varepsilon = 0.001, k_1 = 1, \varepsilon_1 = 0.45, k_2 = 0.75, \varepsilon_2 = 0.45$ (Anderson & Chaplain, 1998), $k_3 = 0.6$ (Abbas et al., 2017), $\varepsilon_3 = 0.01$ (Anderson et al., 2000), $k_4 = 0.8$ (Weidle et al., 2010), $\varepsilon_4 = 0.45$ [present work], $k_5 = 1$ (Cunningham et al., 2010), $\varepsilon_5 = 0.45$ [present work], $k_6 = 1, \varepsilon_6 = 0.01$ (Chaplain & Lolas, 2005) for Case 1. For Case 2, $\varepsilon = 0.0001, \varepsilon_1 = 0.3, \varepsilon_2 = 0.3, \varepsilon_4 = 0.3, \varepsilon_5 = 0.3, \varepsilon_6 = 0.005$ and the remaining parameters were taken as in Case 1. To validate the models, the model presented in Case 1 is compared with the extensions of two other existing models - without drug but with CD147 effects (Sreedaran & Ponnuswamy, 2022) and without drug and without CD147 effects (Anderson & Chaplain, 1998). These extended models are provided in their non-dimensional form as given below. For the case without drug but with CD147 effects, the model is given by

$$\begin{cases} \frac{\partial n}{\partial t} &= D\nabla^2 n - \nabla \cdot \left(\frac{\chi}{1+\alpha c} n \nabla c\right) - \nabla \cdot (\rho n \nabla f) \\ \frac{\partial c}{\partial t} &= -\eta n c + \phi b + \lambda_1 T \\ \frac{\partial f}{\partial t} &= \beta n - \gamma n f - \kappa m f \\ \frac{\partial m}{\partial t} &= D_m \nabla^2 m - \sigma m + \theta b + \lambda_2 T \\ \frac{\partial b}{\partial t} &= D_b \nabla^2 b - \delta b - \psi n b \\ \frac{\partial T}{\partial t} &= D_T \nabla^2 T - \alpha_1 T - \alpha_2 T + \mu(1-b) T \left(1 - \frac{T}{T^*}\right) \end{cases} \quad (16)$$

with the boundary conditions given by

$$\begin{cases} \hat{n} \cdot \left(-D\nabla n + \frac{\chi}{1+\alpha c} n \nabla c + \rho n \nabla f\right) &= 0 \\ \hat{p} \cdot (-D_m \nabla m) &= 0 \\ \hat{q} \cdot (-D_b \nabla b) &= 0 \\ \hat{s} \cdot (-D_T \nabla T) &= 0. \end{cases} \quad (17)$$

The initial conditions for n, c, f, m, b and T are taken as given in Eq. 15 and some of the parameter values for this model are taken to be $\varepsilon_2 = 0.65, \phi = 0.25, \psi = 0.4$ and $\theta = 0.4$. The remaining parameter values are taken from Table 1. For the case without drug and without CD147 effects, the model is given by

$$\begin{cases} \frac{\partial n}{\partial t} &= D\nabla^2 n - \nabla \cdot \left(\frac{\chi}{1+\alpha c} n \nabla c\right) - \nabla \cdot (\rho n \nabla f) \\ \frac{\partial c}{\partial t} &= -\eta n c + \lambda_1 T \\ \frac{\partial f}{\partial t} &= \beta n - \gamma n f - \kappa m f \\ \frac{\partial m}{\partial t} &= D_m \nabla^2 m - \sigma m + \lambda_2 T \\ \frac{\partial T}{\partial t} &= D_T \nabla^2 T - \alpha_1 T - \alpha_2 T + \mu T \left(1 - \frac{T}{T^*}\right). \end{cases} \quad (18)$$

with the boundary conditions given by

$$\begin{cases} \hat{n} \cdot \left(-D\nabla n + \frac{\chi}{1+\alpha c} n \nabla c + \rho n \nabla f\right) &= 0 \\ \hat{p} \cdot (-D_m \nabla m) &= 0 \\ \hat{s} \cdot (-D_T \nabla T) &= 0 \end{cases} \quad (19)$$

The initial conditions for n, c, f, m and T are taken as in Eq. 15 and some of the parameter values for this model are

taken to be $\varepsilon_1 = 0.3, k_3 = 0.33, \kappa = 0.1, \lambda_1 = 0.0001$ and $\lambda_2 = 0.002$ while the remaining parameter values are taken from Table 1.

3. Solution Methodology

The simulation results and graphs are performed using COMSOL Multiphysics 5.4 software (COMSOL, 2023). The generalized mathematical models developed in Section 2 consider a general anti-CD147 drug. To validate the models, a particular anti-CD147 antibody described in the patent by Cunningham et al. is used for the simulations in this paper (Cunningham et al., 2010). The parameter values were borrowed from available literature as much as possible. The parameter values indicated with [present work] are obtained by performing sensitivity analysis. The average values from the sensitivity analysis for each of these parameters are considered in the simulations. The parameters used in the simulations (unless otherwise specified) are given in Table 1. The TAFs and MMPs bind to CD147 receptors present on tumor cell surfaces. The drug acts as a competitive antagonist and binds to the CD147 receptors thus preventing other molecules from binding to the CD147 receptors. Further, there is also the homophilic binding of the cleaved CD147 molecules to the CD147 receptors. Figure 2 illustrates the action of the anti-CD147 drug where the drug binds to the CD147 receptors thereby preventing VEGF and MMPs from binding to the receptors. The drug injection rate is taken in such a way, that the drug will be released at a time $t > t_i$. The drug is considered to be injected after a non-dimensional time $t_i = 5$. Therefore, the results are obtained for times greater than $t = 5$. The drug injection is assumed to be a single administration and the results are obtained for different times t and for different drug doses $1\mu g, 20\mu g$ and $40\mu g$ for the model presented in Case 1 while the drug dose is fixed at 1 μg for the model presented in Case 2.

4. Results and Discussion

4.1 Case 1

Figure 3 shows the migration of ECs without CD147 and without anti-CD147 drug. It is seen that the ECs are moving albeit slowly as compared to that in Anderson and Chaplain (Anderson & Chaplain, 1998). This is because there is no external factor to increase the concentrations of TAFs and MMPs.

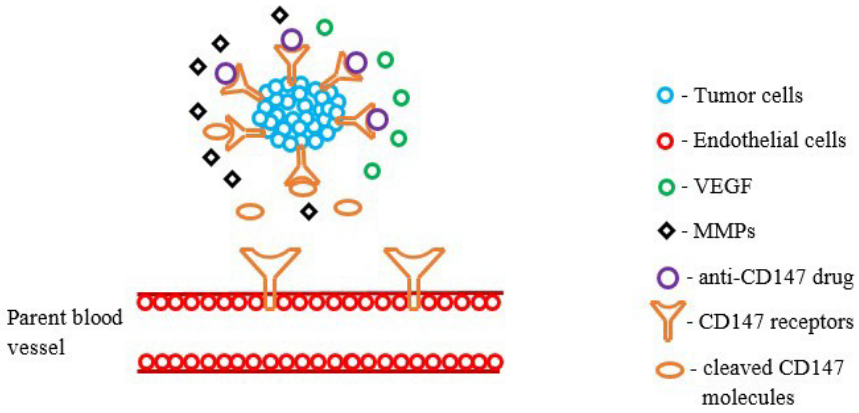

Figure 2: The action of anti-CD147 drug

Table 1(a): Parameter Values

Dimensional Parameter	Description	Dimensional Value	Non-Dimensional	Description
D_n	Diffusion co-efficient of ECs	10^{-10} cm^2 s^{-1}	D	0.00035 (Anderson & Chaplain, 1998)
χ_0	Co-efficient of chemotaxis w.r.t. TAFs	3333.33 m^{2}M^{-1}day^{-1}	χ	0.125 (Addison-Smith, 2010)
k^*	Desensitization parameter	-	ρ	0.6 (Anderson & Chaplain, 1998)
ρ_0	Co-efficient of haptotaxis w.r.t Fibronectin	2666.66 m$^2M^{-1}$day^{-1}		0.1 (Addison-Smith, 2010)
η^*	Uptake rate of TAFs by ECs	3.08645 $\times 10^{-13}$ cm^{3}cell^{-1} s^{-1}	η	0.1 (Anderson & Chaplain, 1998)
λ_1^*	Rate of production of TAFs by tumor cells	-	λ_1	0.02 [present work]

Table 1(b): Parameter Values

Dimensional Parameter	Description	Dimensional Value	Non-Dimensional	Description
β^*	Production rate of fibronectin by ECs	$1.5432 \times 10^{-23}\mathrm{Mcm^3cell^{-1}\ s^{-1}}$	β	0.05 (Anderson & Chaplain, 1998)
γ^*	Uptake rate of fibronectin by ECs	$3.08645 \times 10^{-13}\ \mathrm{cm^3cell^{-1}\ s^{-1}}$	γ	0.1 (Anderson & Chaplain, 1998)
D_m^*	Diffusion co-efficient of MMPs	$1.3729 \times 10^{-8}\ \mathrm{cm^2\ s^{-1}}$	D_m	0.04448 (Collier et al., 2011)
σ^*	Decay rate of MMPs	$5.321 \times 10^{-6}\ \mathrm{s^{-1}}$	σ	0.6896 (Jiang et al., 2014)
κ^*	Uptake rate of fibronectin by MMPs	$370\ \mathrm{cm^3\ g^{-1}\ s^{-1}}$	κ	1 (Franssen et al., 2019)
λ_2^*	Rate of production of MMPs by tumor cells		λ_2	0.00143856 (Kim et al., 2009)
D_b^*	Diffusion co-efficient of CD147	$0.237 \times 10^{-8}\ \mathrm{cm^2\ s^{-1}}$	D_b	0.0076788 (Wieser et al., 2009)
δ^*	Decay rate of CD147	$1.3832 \times 10^{-5}\ \mathrm{s^{-1}}$	δ	1.7926 (Xiao & Wu, 2017)
D_d^*	Diffusion co-efficient of anti-CD147 drug	-	D_d	1.6 [present work]
ω^*	Decay rate of anti-CD147 drug	$0.033007\mathrm{day^{-1}}$	ω	0.0495 (Tseng et al., 2020)
D_T^*	Diffusion co-efficient of tumor cells	$4.32 \times 10^{-6}\ \mathrm{cm^2\ day^{-1}}$	D_T	0.0001724 (Liao et al., 2014)
α_1^*	Necrosis rate of tumor cells	$8.3 \times 10^{-1}\mathrm{day^{-1}}$	α_1	1.245 (Liao et al., 2014)
α_2^*	Apoptosis rate of tumor cells	$4.15 \times 10^{-1}\mathrm{day^{-1}}$	α_2	0.6225 (Liao et al., 2014)
μ^*	Proliferation rate of tumor cells	$2.5\mathrm{day^{-1}}$	μ	3.75 (Liao et al., 2014)
T_0^*	Carrying capacity of tumor cells	$10^9\ \mathrm{cell\ cm^{-3}}$	T^*	1.38888 (Liao et al., 2014)
$E_{\max_c}$	Maximum effect of TAFs on chemotaxis	-	$E_{\max_c}$	1 (Barleon et al., 1996)
$E_{\max_{b,c}}$	Maximum effect of CD1 147 on TAFs	-	$E_{\max_{b,c}}$	0.925 (Cunningham et al., 2010)
$E_{\max_{b,m}}$	Maximum effect of CD147 on MMPs	-	$E_{\max_{b,c}}$	0.95 (Cunningham et al., 2010)
$E_{\max_{b,T}}$	Maximum effect of CD147 on tumor cells	-	$E_{\max_{b,T}}$	0.75 (Wang et al., 2010; Yin et al., 2017)
$B_{\max\ b}$	Maximum binding of CD147		$B_{\max\ b}$	3.095 (Sagert et al., 2018)
$B_{\max\ d}$	Maximum binding of anti-CD147 drug	-	$B_{\max\ d}$	3.095 (Sagert et al., 2018)
$K_{D_{b,c}}^*$	Equilibrium dissociation constant of CD147 w.r.t. TAFs	40 pM	$K_{D_{b,c}}^*$	0.04 (Li et al., 2002)
$K_{D_{b,m}}^*$	Equilibrium dissociation constant of CD147 w.r.t MMPs	$0.187\mu M$	$K_{D_{b,m}}^*$	0.19303 (Wu et al., 2013)
$K_{D_{b,b}}^*$	Homophilic dissociation constant of CD147	$40\mu M$	$K_{D_{b,b}}^*$	0.289855 (Hanna et al., 2003)
$K_{D_{b,d}}^*$	Equilibrium dissociation constant of CD147 w.r.t anti-CD147 drug	0.46 nM	$K_{D_{b,d}}^*$	0.046 (Cunningham et al., 2010)
$K_{D_{d,c}}^*$	Equilibrium dissociation constant of anti-CD147 drug w.r.t TAFs	0.46 nM	$K_{D_{d,c}}^*$	0.046 (Cunningham et al., 2010)
$K_{D_{d,m}}^*$	Equilibrium dissociation constant of anti-CD147 drug w.r.t MMPs	$0.46nM$	$K_{D_{d,m}}^*$	0.046 (Cunningham et al., 2010)
$K_{D_{d,b}}^*$	Equilibrium dissociation constant of anti-CD147 drug w.r.t CD147	0.46 nM	$K_{D_{d,b}}^*$	0.046 (Cunningham et al., 2010)

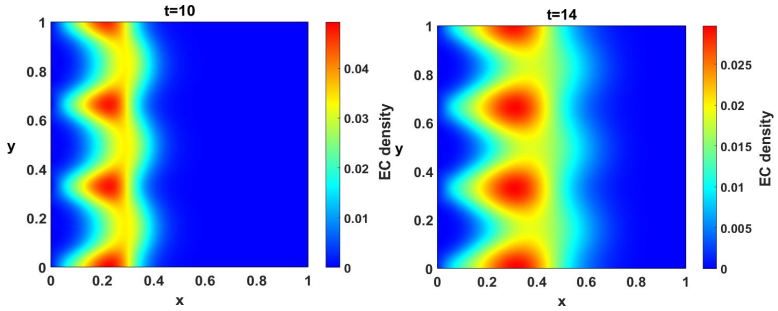

(a) (b)

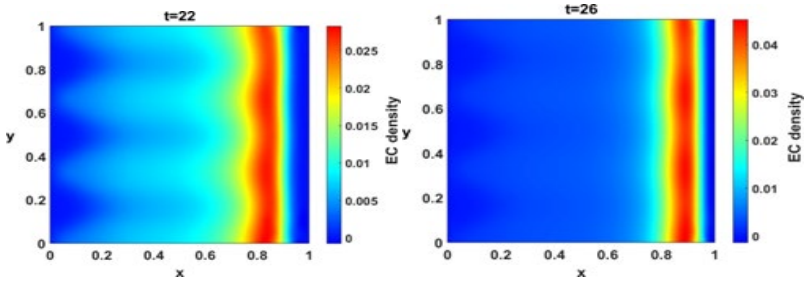

(c) (d)

Figure 3: The migration of ECs at time (a) $t = 10$, (b) $t = 14$, (c) $t = 22$ and (d) $t = 26$ in the absence of anti-CD147 drug and absence of CD147

The ECs have moved up to $x = 0.5$ at time $t = 14$. As the time is increased, the ECs have reached $x = 0.9$ at time $t = 22$ and when the time is further increased, the ECs are almost close to the tumor at $t = 26$.

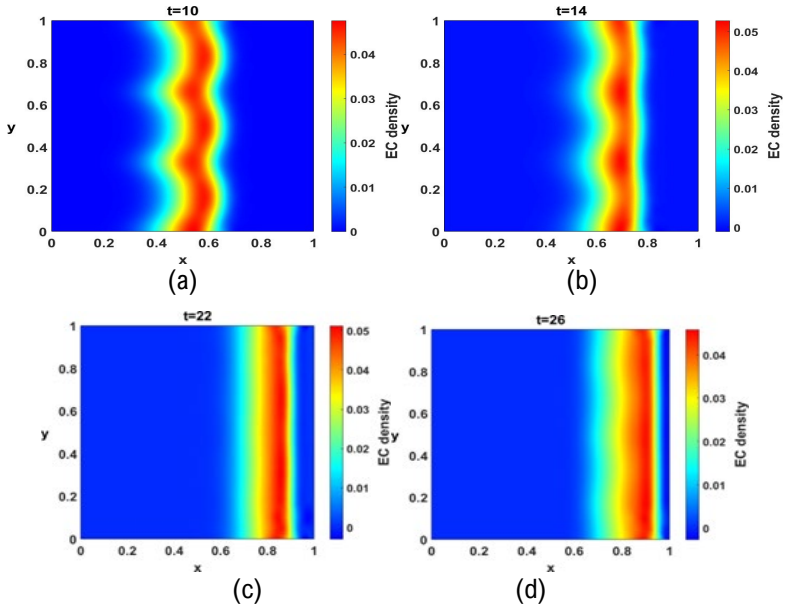

(a) (b)

(c) (d)

Figure 4: The migration of ECs at time (a) $t = 10$, (b) $t = 14$, (c) $t = 22$ and (d) $t = 26$ under the presence of CD147 and in the absence of anti-CD147 drug

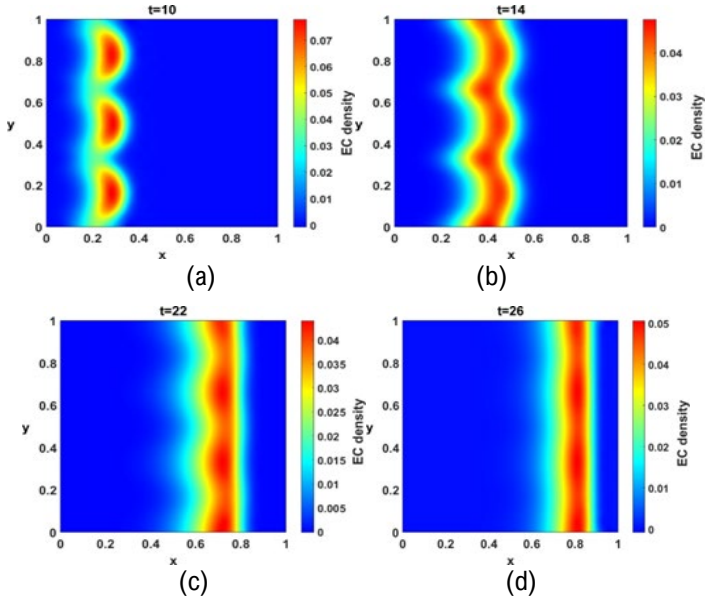

(a) (b)

(c) (d)

Figure 5: The EC migration for drug dose 1 μg at times (a) $t = 10$, (b) $t = 14$, (c) $t = 22$ and (d) $t = 26$

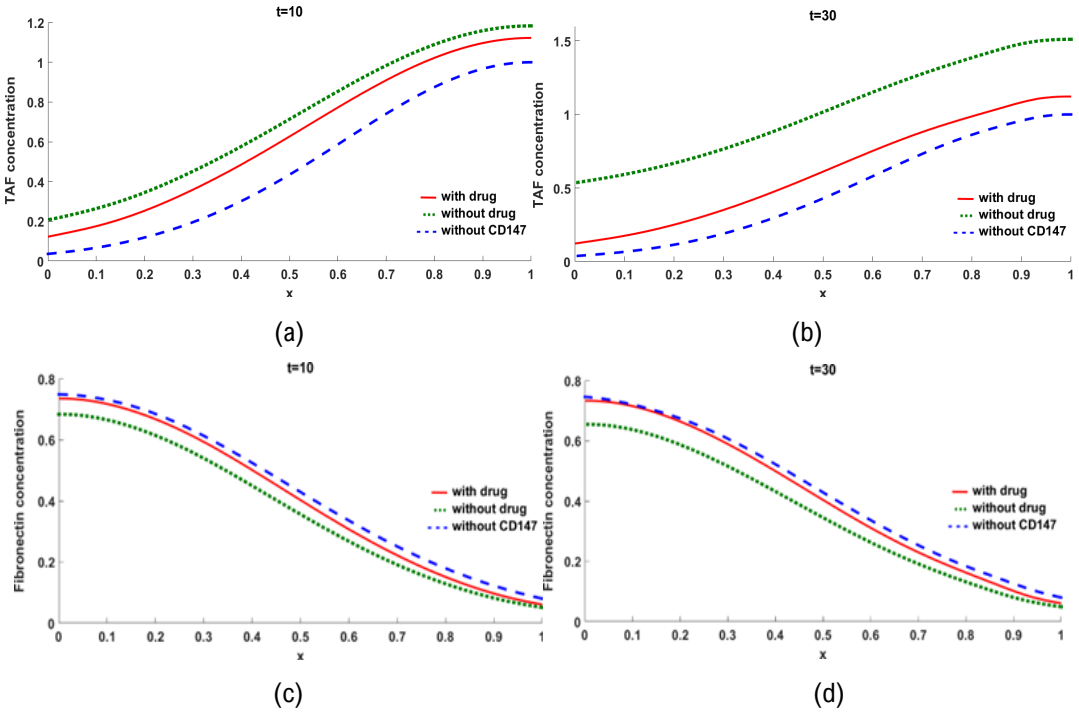

Figure 6: The concentration of TAFs for without CD147, without drug and with drug at time (a) $t = 10$, (b) $t = 30$ and fibronectin concentration at time (c) $t = 10$ and (d) $t = 30$

Figure 4 shows the EC migration when there is no action of the anti-CD147 drug but under the action of CD147. It is seen that the ECs move faster towards the tumor under the action of CD147 as compared to Figure 3. This is due to the fact that CD147 increases TAFs and MMPs (Wang et al., 2016) which in turn increases chemotaxis effect and hence increases endothelial cell motility. The migration of ECs is very rapid and it is seen that the ECs have moved almost near to the tumor by the time $t = 26$. The graphs in Figure 5, show the movement of the ECs for different times with drug dose $1\mu g$. From Figure 5, the ECs are seen to be moving towards the tumor as the time increases. Initially, the motion of the ECs is similar to that in the case without the effect of CD147 (Figure 3). However, the speed at which the ECs move has been reduced due to the effect of the anti-CD147 drug as compared to Figure 4. The TAFs and MMPs bind to CD147 receptors and these bindings are prevented by the drug which competes to bind to the CD147 receptors. This prevents the increase in TAFs and MMPs caused due to CD147. This in turn prevents rapid motion of the ECs towards the tumor and thus the ECs move slower due to the action of the drug. However, as the time progresses, the pace of the ECs pick up and they move towards the tumor. This will eventually lead to angiogenesis. This prompts for increasing the dose of the drug to prevent the ECs from reaching the tumor. The graphs of other concentrations for the cases with drug ($1\mu g$), without drug (but with CD147) and without CD147 effects are also considered. Figure 6 shows the concentrations of TAFs and fibronectin under all three cases for two different times $t = 10$ and $t = 30$. It is seen that the anti-CD147 drug reduces the TAF concentration as compared to the case without drug but with CD147. When CD147 is not involved, the concentration is much less than the other two cases. The drug is not directly applied to fibronectin. It depends on ECs, TAFs and MMPs where the drug is applied and there is an effect produced in the fibronectin concentration. It is seen from the graphs that the fibronectin concentration is higher in the absence of CD147 but is reduced in the presence of CD147. When the anti-CD147 drug is applied, there is an increase in the fibronectin concentration as compared with the no-drug case. Figure 7 presents the graphs for cases with the presence of anti-CD147 drug $(1\mu g)$, absence of anti-CD147 drug but the presence of CD147 and absence of CD147 for MMP concentration. The figure 7 also presents he graphs for CD147 concentration under the presence and absence of the drug. Figures 7(a) and 7(b) show the concentrations of MMPs at times $t = 7$ and $t = 10$. It is seen from the graphs that the drug reduces the MMP concentration as compared to the case without drug and in the absence of CD147, the MMP concentration is low since there is no external stimulating factor to induce MMPs. Figure 7(c) and 7(d) contains graphs for the concentration of CD147 under the presence and absence of anti-CD147 drug at times $t = 6$ and $t = 8$. The graphs indicate that there is a reduction in the CD147 concentration under the action of the drug as compared with the case of no-drug. This is due to the binding effect the drug has on CD147. Figure 8 gives the graphs of tumor cell density for cases with the presence of anti-CD147 drug ($1\mu g$), absence of anti-CD147 drug but the

presence of CD147 and absence of CD147 for times $t = 7$ and $t = 10$. It is seen that there is reduction in the density of tumor cells as the time progresses. This is due to the drug applied to curb the proliferation of tumor cells and this strategy seems to be effective as seen from the graphs. It is seen from Figure 5 that there is a need to increase the dose of the anti-CD147 drug for effective curbing of angiogenesis. Hence, the drug dose is increased to $20\mu g$ and $40\mu g$. Figures 9 and 10 show the motion of the ECs at various times and with drug doses $20\mu g$ and $40\mu g$ respectively. As the dose of the drug is increased, there is a reduction in the pace of the ECs as compared to that with dose $1\mu g$. The reduction is not clearly noticeable in the initial stages, but as the time increases, the pace reduction of the ECs is seen clearly. At time $t = 14$, the ECs have moved up to $x = 0.4$ while that in the lower dose have moved up to $x = 0.5$. For the time $t = 22$, the ECs have moved up to $x = 0.7$ as compared to that with dose $1\mu g$ in which the ECs have moved up to $x = 0.8$. At time $t = 26$, the ECs, have moved up to $x = 0.8$ as compared to dose $1\mu g$ where the ECs have moved up to $x = 0.9$. The change of dose from $20\mu g$ to $40\mu g$ has a negligible effect on the motion of the ECs. However, there is a set-back in the angiogenesis process in the drug dose from $1\mu g$ to $20\mu g$ as compared with Anderson and Chaplain (Anderson & Chaplain, 1998). The inclusion of the drug effect to the angiogenesis model given in Anderson and Chaplain (Anderson & Chaplain, 1998) along with the effects of other factors like MMPs and their inhibition due to the drug, gives an edge to how angiogenesis can be delayed. The results in Figure 9 show that there is regression of the vasculature as CD147 concentration is reduced and this is in accordance with the results presented in Voigt et al. (Voigt et al., 2009) and Xiong et al. (Xiong et al., 2016). The effect of the drug on other quantities is also presented. Figures 11, 12 and 13 shows the effect of the drug dose on the concentrations of TAFs, fibronectin, MMPs, CD147 and tumor cell density. It is seen from Figure 11(a), that an increase in the drug dose reduces the TAF concentration. The reduction is high when considering doses $1\mu g$ and $20\mu g$. However, there is less reduction when considering doses $20\mu g$ and $40\ \mu g$. Figure 11(b) indicates an increase in fibronectin concentration as drug dose increases. The increase is not high but it is noticeable from dosage $1\mu g$ to dose $20\mu g$. The concentration for doses $20\mu g$ and $40\mu g$ coincides indicating that saturation is attained.

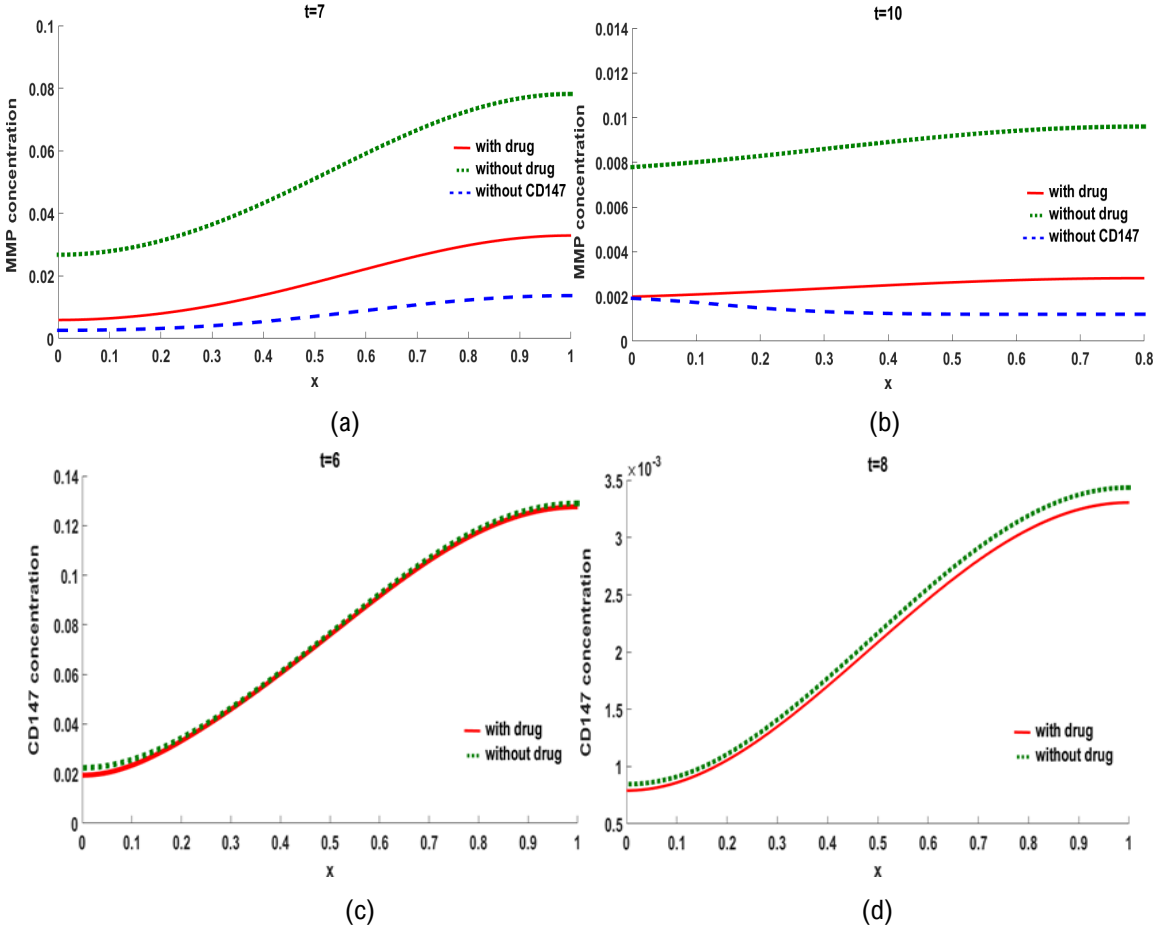

Figure 7: The concentration of MMPs for without CD147, without drug and with drug at time (a) $t = 7$, (b) $t = 10$ and the concentration of CD147 with drug and without drug at time (c) $t = 6$ and (d) $t = 8$

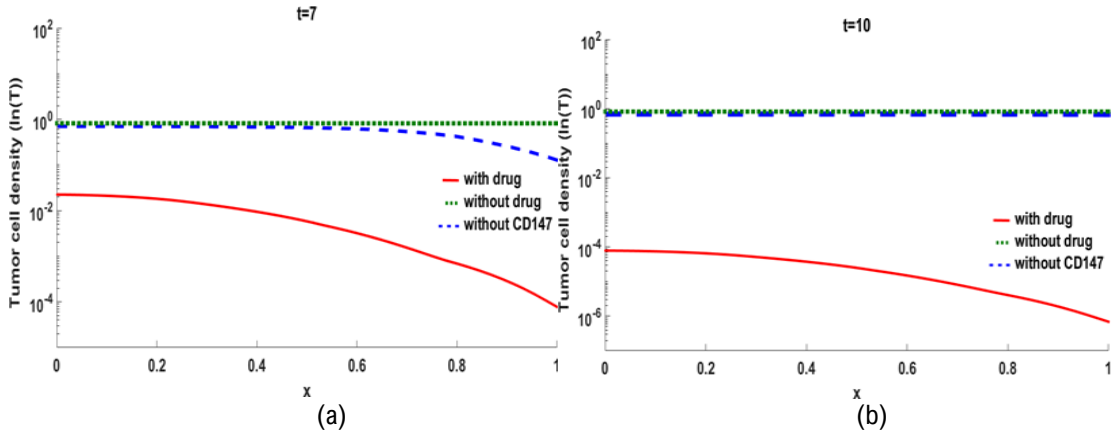

Figure 8: The density of tumor cells for without CD147, without drug and with drug at time (a) $t = 7$ and (b) $t = 10$

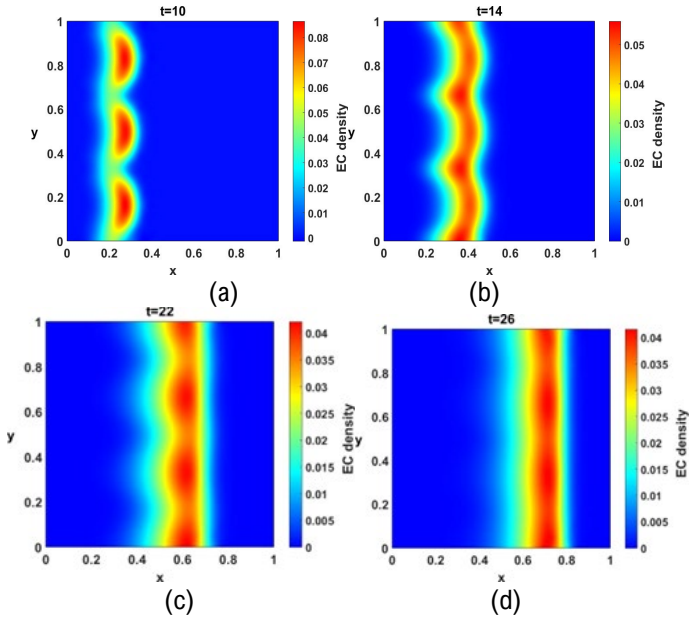

Figure 9: The EC migration for drug dose 20 μg at times (a) $t = 10$, (b) $t = 14$, (c) $t = 22$ and (d) $t = 26$

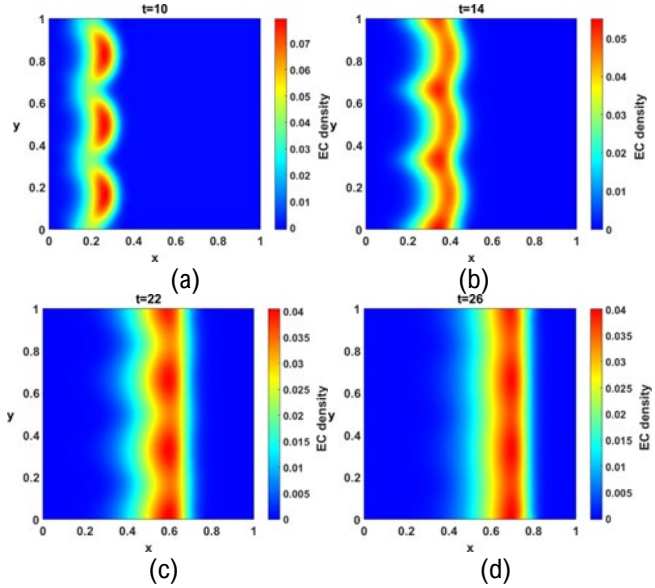

Figure 10: The EC migration for drug dose 40 μg at times (a) $t = 10$, (b) $t = 14$, (c) $t = 22$ and (d) $t = 26$

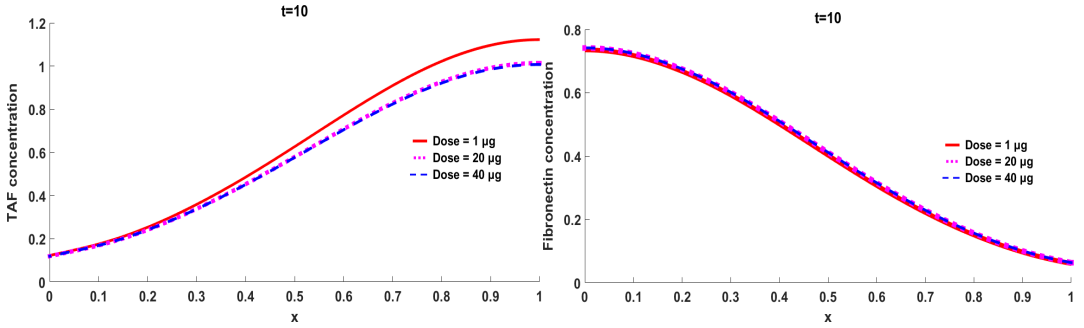

(a) (b)

Figure 11: The impact of different drug doses on (a) TAF concentration and (b) Fibronectin concentration

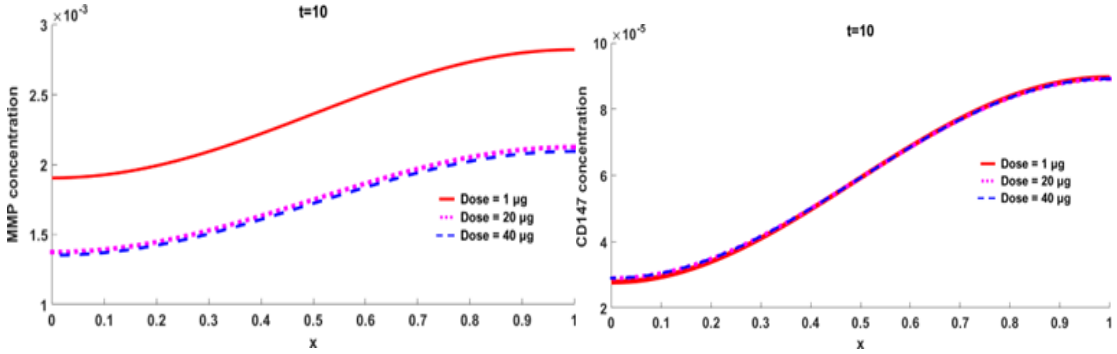

(a) (b)

Figure 12: The impact of different drug doses on (a) MMP concentration and (b) CD147 concentration

Figure 12(a) shows a decreasing trend for MMP concentration as drug dose increases. There is a drastic decrease in MMP concentration from dose $1\mu g$ to dose $20\mu g$. There is also a reduction in concentration from dose $20\mu g$ to dose $40\mu g$, but the decrease is low. It is seen from Figure 12(b) that there is negligible change in the CD147 concentration due to increase in the drug dose. From Figure 13, it is seen that there is reduction in the tumor cell density as the drug dose increases from $1\mu g$ to $20\mu g$, but the reduction is low. For drug doses $20\mu g$ and $40\mu g$, the graph for the density of tumor cells coincides. The effect of the drug dose on tumor cell proliferation is negligible indicating that the saturation has occurred.

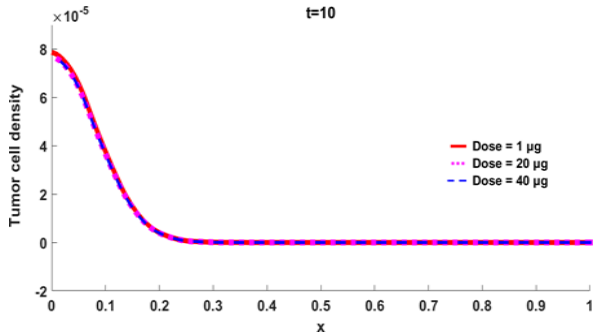

Figure 13: The impact of different drug doses on the density of tumor cells

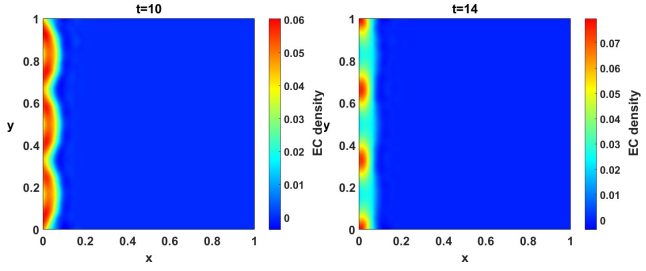

(a) (b)

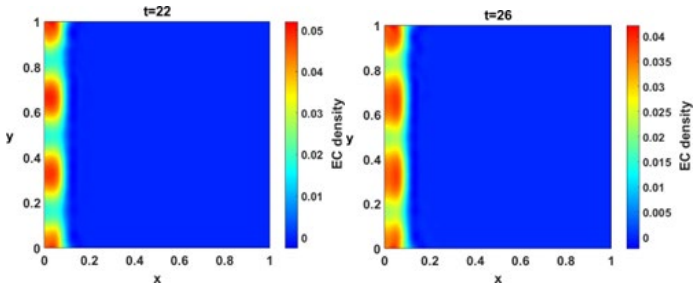

(c) (d)

Figure 14: The migration of ECs at time (a)t = 10, (b)t = 14, (c)t = 22 and (d)t = 26 for Case 2

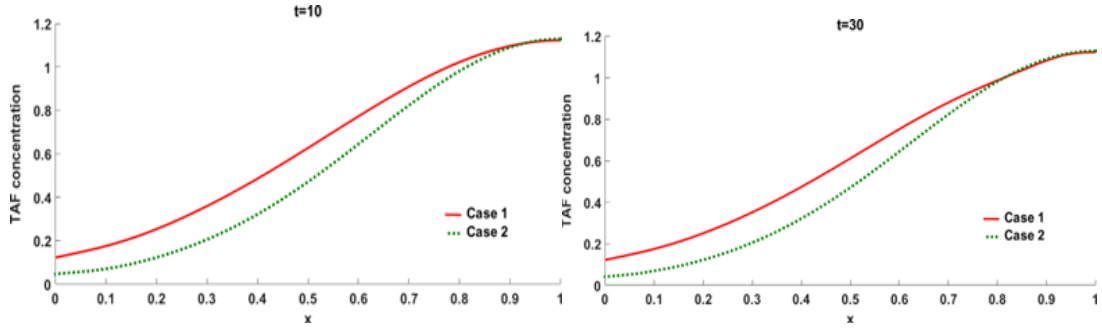

(a) (b)

Figure 15: The concentration of TAFs for Case 1 and Case 2 at times (a) t = 10, (b) t = 30

4.2 Case 2

The graphs pertaining to the effect of the drug that is directly applied on the EC chemotaxis are presented in Figure 14, keeping the drug dose fixed at $1\mu g$. The plots show the migration of ECs for different times for Case 2. It is seen that the ECs move very slowly from the parent vessel situated at $x = 0$ towards the tumor situated at $x = 1$. As the time increases, it is seen that the movement of the ECs is curtailed by the action of the drug and the ECs have moved only up to $x = 0.1$ even at time $t = 26$. This is due to the action of the anti-CD147 drug on TAFs and MMPs. However, the drug is also applied to chemotaxis (cell migration) and this curbs the endothelial cell migration to a great extent as compared to Case 1 (Figure 5). The effect of the drug on other quantities is also presented for Case 2 and the graphs are compared with that of Case 1 (with drug dose $1\mu g$). Figure 15 shows the graphs pertaining to the concentration of TAFs at times $t = 10$ and $t = 30$. It is seen that there is a reduction the concentration of TAFs in Case 2 as compared to Case 1. The TAFs are secreted by the tumor (at the boundary $x = 1$) and then they are taken up the ECs (moving from the boundary $x = 0$). This uptake of TAFs by the ECs is higher in Case 2 resulting in the decline of the TAF concentration in Case 2 as compared to Case 1. Figure 16 shows the graphs pertaining to the concentration of fibronectin at times $t = 10$ and $t = 30$. It is seen that there is a reduction the concentration of fibronectin in Case 2 as compared to Case 1. The fibronectin is produced by the ECs (at the boundary $x = 0$) and then they are taken up the ECs (moving from the boundary $x = 0$ towards the boundary $x = 1$). This uptake of fibronectin by the ECs is higher in Case 2 resulting in the decline of the fibronectin concentration in Case 2 as compared to Case 1.

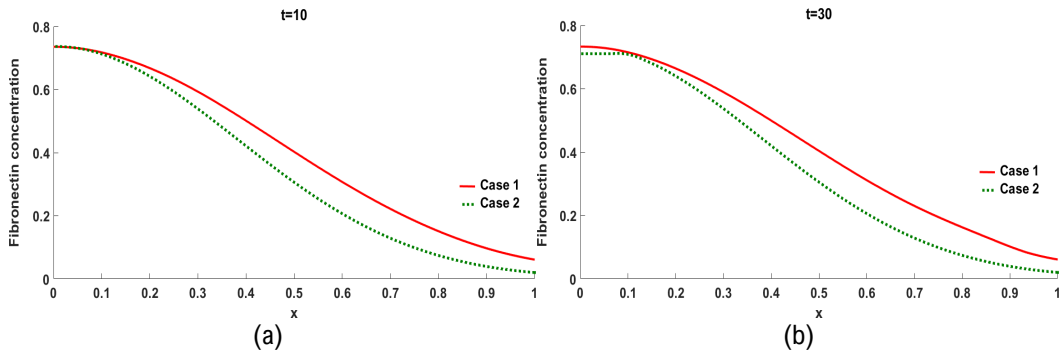

(a) (b)

Figure 16: The concentration of fibronectin for Case 1 and Case 2 at times (a) t = 10, (b) t = 30

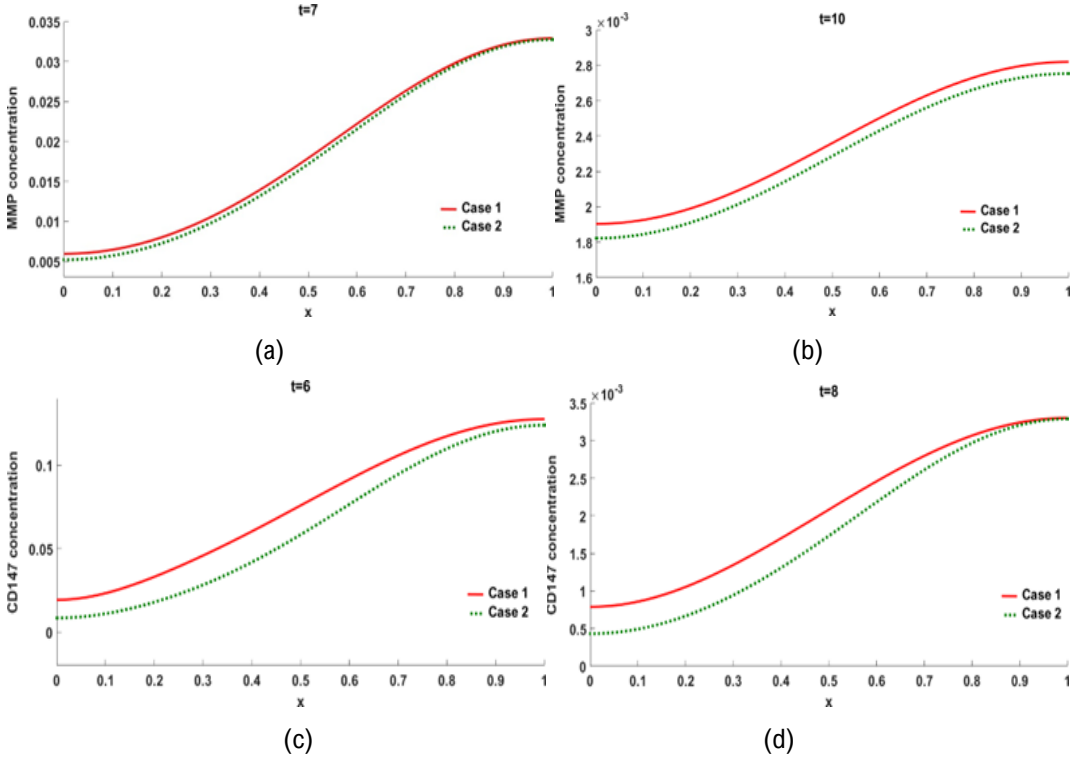

Figure 17: The concentration of MMPs for Case 1 and Case 2 at times (a) $t = 7$, (b) $t = 10$ and the concentration of CD147 for Case 1 and Case 2 at times (c) $t = 6$ and (d) $t = 8$

Figure 17 presents the graphs for the concentration of MMPs at times $t = 7$ and $t = 10$ and CD147 concentration at times $t = 6$ and $t = 8$. It is observed that there is a decrease in the concentration of both MMPs and CD147 in Case 2 as compared to Case 1. Figure 18 presents the graphs for tumor cell density at times $t = 7$ and $t = 10$. There is a decrease in the tumor cell density in the initial stage, for Case 2 as compared to Case 1, before attaining saturation. The reduction of the concentrations of TAFs, fibronectin, MMPs, CD147 and tumor cell density in Case 2 is due to the application of the anti-CD147 drug which is directly applied to the EC chemotaxis which in turn impacts the concentrations of the other variables.

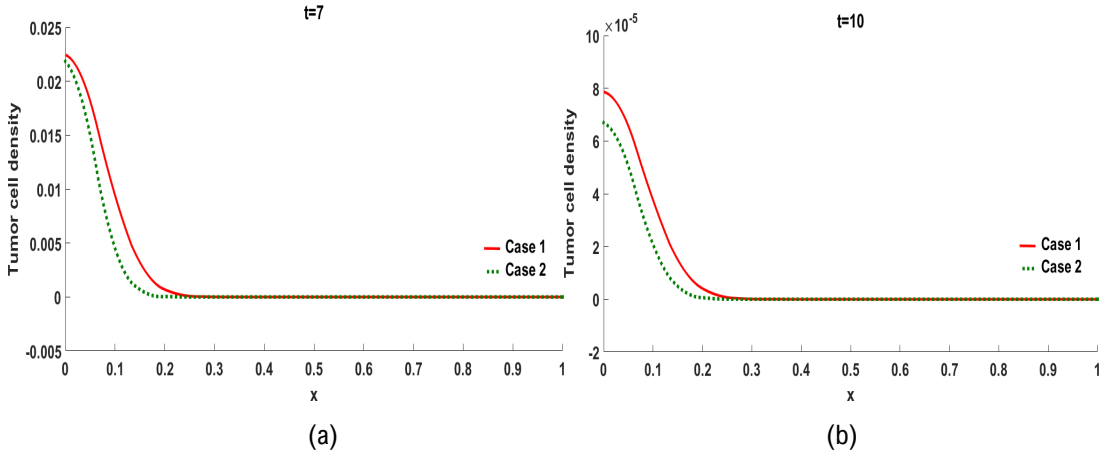

Figure 18: The tumor cell density for Case 1 and Case 2 at times (a) $t = 7$ and (b) $t = 10$

5. Conclusions and Future Work

The focus of this research is to prevent or delay the tumor angiogenesis process. It has been found that CD147 increases and induces VEGF and MMPs (Wang et al., 2016), thus aiding in the angiogenesis process. To prevent the effects of CD147 on angiogenesis, anti-CD147 drug is used. The effect of a general anti-CD147 drug on tumor angiogenesis is studied with the help of mathematical models. The novelty of this paper is the inclusion of a general anti-CD147 drug

concentration and its effects on various quantities like TAFs, MMPs and tumor cell density and also on cell migration. The effects of the drug are considered through drug-receptor binding kinetics and with the use of the classical $E_{\max}$ model. The anti-CD147 drug is modeled with the assumption that it is a competitive antagonist which competes with TAFs and MMPs to bind to the CD147 receptor. This results in the prevention of TAFs and MMPs from binding to CD147 receptor. The effects of a particular anti-CD147 drug on ECs, TAFs, MMPs, fibronectin, CD147 and on tumor cells are discussed. The results are obtained in the presence and absence of the antiCD147 drug and also in the absence of CD147. The results show that there is a decrease in the TAF and MMP concentrations when the drug is applied in the model for Case 1 (dose $1\mu g$) as compared to the no-drug case. The results also show an increase in the fibronectin concentration due to the indirect effect of the drug. The CD147 concentration is also reduced due to the binding of the drug. The tumor proliferation is also subjected to the drug action and it is seen that there is an overall reduction in the tumor cell density. There is also a reduction in the speed of the ECs as a consequence of the drug as compared to the no-drug case. The conditions for drug doses are also explored. As the drug dose increases from $1\mu g$ to $20\mu g$, it is seen that there is a reduction in TAF and MMP concentrations, which greatly reduces the motion of the ECs towards the tumor. The change in the drug dose has minimal effect on other quantities. As expected, it is seen from the results that higher the dose $(20\mu g)$, more is the inhibition rate of angiogenesis. There is a regression of the vasculature due to the CD147 knockdown effect (with the help of the anti-CD147 drug) which is in accordance with the experimental results presented in Voigt et al. (Voigt et al., 2009) and Xiong et al. (Xiong et al., 2016). It is also observed that there is a negligible change of the effects beyond $20\mu g$ drug dose indicating that saturation of the effects has occurred.

Further, the anti-CD147 drug is applied directly to EC chemotaxis in Case 2. It is known that the TAFs are the major driving force for angiogenesis (Khayati et al., 2015). Therefore, chemotaxis, the process of endothelial cell migration towards TAFs, dominate over other aspects. Hence, the drug effect is modeled and applied to the chemotaxis term using the $E_{\max}$ model. In Case 1, it is seen that the dose has to be increased in order to curb the migration of ECs towards the tumor. However, the drug dose of $1\mu g$ in Case 2 is sufficient to reduce the migration of ECs to a large extent. The ECs are seen to be migrating very slowly and have moved only up to $x = 0.1$ even at time $t = 26$ (39 days) and this is because the dominant chemotaxis effect is subjected to the action of the anti-CD147 drug. This is a major novel finding of this research. Thus, this model effectively delays the tumor angiogenesis process. The results are in agreement with the experimental results presented by Khayati et al. (Khayati et al., 2015) and Voigt et al. (Voigt et al., 2009). It is clear from Case 2 that application of the anti-CD147 drug on EC chemotaxis is an effective way to curb angiogenesis. The models presented here considered a generalized anti-CD147 drug and used to help in delaying the angiogenesis process. Although the study presented promising results to curb angiogenesis, one needs to proceed with caution towards using anti-angiogenesis treatment alone. There are drawbacks associated with anti-angiogenic treatments as presented by Ribatti et al. (Ribatti et al., 2019). The major drawbacks associated with anti-CD147 drug treatment is that the drug induces hypoxia as it reduces VEGF expression. The resulting hypoxia (or inadequate oxygen supply) is caused when the drug is applied for a prolonged time. Further, the reduction in VEGF results in the tumor using other methods for vascular growth like vascular intussusception and vascular mimicry (Ribatti et al., 2019). It has also been found that the knockdown of CD147 expression leads to increase in β-amyloid peptides which leads to formation of plaques and Alzheimer disease. The knockdown of CD147 also causes damage to the retina (Koltai et al., 2020). In the clinical scenario, it is highly unlikely to apply only anti-CD147 drug treatment. However, this treatment option would work much effectively in curbing angiogenesis and reducing the risk factors associated with it, if it is used as a combinatorial therapy alongside other therapeutic models like chemotherapy (Rataj, 2014). Future work could explore the optimal drug dosage regimens. Also, the inclusion of other properties of CD147 - like hyaluronan production, Warburg effect etc. and targeting such properties with suitable drugs along with other combinatorial treatment modalities might provide a better treatment strategy for preventing tumor angiogenesis.

6. Acknowledgement

The authors profusely thank the reviewers, the Associate Editors and the Editor in Chief for their valuable comments which have helped in improvising the manuscript to a great extent.

7. References

Abbas, N. F., Shabana, M. E.-A., Habib, F. M., & Soliman, A. A. (2017). Histopathological and immunohistochemical study of matrix metalloproteinase-2 and matrix metalloproteinase-9 in breast carcinoma. *Journal of The Arab Society for Medical Research*, *12*(1), 6-12.

Addison-Smith, E. A. (2010). *Mathematical modelling of tumour-induced angiogenesis* Queensland University of

Technology].

Amit-Cohen, B.-C., Rahat, M. M., & Rahat, M. A. (2013). Tumor cell-macrophage interactions increase angiogenesis through secretion of EMMPRIN. *Frontiers in physiology*, *4*, 178.

Anderson, A. R., & Chaplain, M. A. (1998). Continuous and discrete mathematical models of tumor-induced angiogenesis. *Bulletin of mathematical biology*, *60*(5), 857-899.

Anderson, A. R., Chaplain, M. A., Newman, E. L., Steele, R. J., & Thompson, A. M. (2000). Mathematical modelling of tumour invasion and metastasis. *Computational and Mathematical Methods in Medicine*, *2*(2), 129-154.

Barleon, B., Sozzani, S., Zhou, D., Weich, H. A., Mantovani, A., & Marme, D. (1996). Migration of human monocytes in response to vascular endothelial growth factor (VEGF) is mediated via the VEGF receptor flt-1.

Billy, F., Ribba, B., Saut, O., Morre-Trouilhet, H., Colin, T., Bresch, D., Boissel, J.-P., Grenier, E., & Flandrois, J.-P. (2009). A pharmacologically based multiscale mathematical model of angiogenesis and its use in investigating the efficacy of a new cancer treatment strategy. *Journal of theoretical biology*, *260*(4), 545-562.

Cai, Y., Zhang, J., & Li, Z. (2016). Multi-scale mathematical modelling of tumour growth and microenvironments in anti-angiogenic therapy. *Biomedical Engineering Online*, *15*, 685-700.

Chaplain, M., & Lolas, G. (2005). Mathematical modelling of cancer cell invasion of tissue: The role of the urokinase plasminogen activation system. *Mathematical Models and Methods in Applied Sciences*, *15*(11), 1685-1734.

Chen, J., Pan, Y., He, B., Ying, H., Wang, F., Sun, H., Deng, Q., Liu, X., Lin, K., & Peng, H. (2015). Inhibition of CD147 expression by RNA interference reduces proliferation, invasion and increases chemosensitivity in cancer stem cell-like HT-29 cells. *International journal of oncology*, *47*(4), 1476-1484.

Chen, Y., Gou, X., Ke, X., Cui, H., & Chen, Z. (2012). Human tumor cells induce angiogenesis through positive feedback between CD147 and insulin-like growth factor-I. *PloS one*, *7*(7), e40965.

Collier, I. E., Legant, W., Marmer, B., Lubman, O., Saffarian, S., Wakatsuki, T., Elson, E., & Goldberg, G. I. (2011). Diffusion of MMPs on the surface of collagen fibrils: the mobile cell surface–collagen substratum interface. *PloS one*, *6*(9), e24029.

COMSOL, M. (2023). 'Products'. https://www.comsol.com/products

Cunningham, M. J., Behzadi, S., Tang, Y., & Van, L. (2010). *Anti-CD147 antibodies, methods and uses*.

Dick, R. M. (2011). Chapter 2. Pharmacodynamics: The Study of Drug Action. *Ouellette R, Joyce JA. Pharmacology for Nurse Anesthesiology. Jones & Bartlett Learning*, 17-26.

Folkman, J. (1971). Tumor angiogenesis: therapeutic implications. *N Engl j Med*, *285*(21), 1182-1186.

Folkman, J. (1972). Anti-angiogenesis: new concept for therapy of solid tumors. *Annals of surgery*, *175*(3), 409-416.

Franssen, L. C., Lorenzi, T., Burgess, A. E., & Chaplain, M. A. (2019). A mathematical framework for modelling the metastatic spread of cancer. *Bulletin of mathematical biology*, *81*, 1965-2010.

Hanna, S. M., Kirk, P., Holt, O. J., Puklavec, M. J., Brown, M. H., & Barclay, A. N. (2003). A novel form of the membrane protein CD147 that contains an extra Ig-like domain and interacts homophilically. *BMC biochemistry*, *4*, 1-9.

Hatanaka, M., Higashi, T., Shibuya, T., Takah, N., Kiwa, E., Hashiguchi, T., Seno, K., Zheng, W., Chen, X., & Kaneko, K. (2019). Identification of the chemical structure of antiangiogenic drugs that activates MMP2, VEGF and CD147 pathways. *Nature Biotechnology*, *37*(1), 122–126.

Jiang, C., Cui, C., Li, L., & Shao, Y. (2014). The anomalous diffusion of a tumor invading with different surrounding tissues. *PloS one*, *9*(10), e109784.

Khayati, F., Pérez-Cano, L., Maouche, K., Sadoux, A., Boutalbi, Z., Podgorniak, M.-P., Maskos, U., Setterblad, N., Janin, A., & Calvo, F. (2015). EMMPRIN/CD147 is a novel coreceptor of VEGFR-2 mediating its activation by VEGF. *Oncotarget*, *6*(12), 9766.

Kim, Y., Lawler, S., Nowicki, M. O., Chiocca, E. A., & Friedman, A. (2009). A mathematical model for pattern formation of glioma cells outside the tumor spheroid core. *Journal of theoretical biology*, *260*(3), 359-371.

Koltai, T., Reshkin, S. J., & Harguindey, S. (2020). *An innovative approach to understanding and treating cancer: targeting*

ph: from etiopathogenesis to new therapeutic avenues. Academic Press.

Krzyzanski, W. (2013). Systems pharmacology models for guiding drug design. *CPT: Pharmacometrics & Systems Pharmacology*, *2*(4), e39.

Leber, M. F., & Efferth, T. (2009). Molecular principles of cancer invasion and metastasis. *International journal of oncology*, *34*(4), 881-895.

Li, B., Ogasawara, A. K., Yang, R., Wei, W., He, G.-W., Zioncheck, T. F., Bunting, S., de Vos, A. M., & Jin, H. (2002). KDR (VEGF receptor 2) is the major mediator for the hypotensive effect of VEGF. *Hypertension*, *39*(6), 1095-1100.

Liao, K.-L., Bai, X.-F., & Friedman, A. (2014). Mathematical modeling of Interleukin-35 promoting tumor growth and angiogenesis. *PloS one*, *9*(10), e110126.

Lupo, G., Caporarello, N., Olivieri, M., Cristaldi, M., Motta, C., Bramanti, V., Avola, R., Salmeri, M., Nicoletti, F., & Anfuso, C. D. (2017). Anti-angiogenic therapy in cancer: downsides and new pivots for precision medicine. *Frontiers in pharmacology*, *7*, 519.

Oduola, W. O., & Li, X. (2018). Multiscale tumor modeling with drug pharmacokinetic and pharmacodynamic profile using stochastic hybrid system. *Cancer Informatics*, *17*, 1176935118790262.

Paweletz, N., & Knierim, M. (1989). Tumor-related angiogenesis. *Critical reviews in oncology/hematology*, *9*(3), 197-242.

Rataj, F. (2014). *A novel multi-target cancer therapy based on destabilization of short-lived mRNAs* Université de Grenoble].

Ribatti, D., Annese, T., Ruggieri, S., Tamma, R., & Crivellato, E. (2019). Limitations of anti-angiogenic treatment of tumors. *Translational Oncology*, *12*(7), 981-986.

Rundhaug, J. E. (2005). Matrix metalloproteinases and angiogenesis. *Journal of cellular and molecular medicine*, *9*(2), 267-285.

Sagert, J. G., Lin, S. J., West, J. W., & Terrett, J. A. (2018). Cd147 antibodies, activatable cd147 antibodies, and methods of making and use thereof. In: Google Patents.

Salhabdeen, M. S., & Niahsitha, P. S. (2017). An overview of pharmacodynamics modeling, ligand-binding analysis, and small-molecule drug design. *Frontiers of Pharmacological Journal*, *87*(5), 160–178.

Sreedaran, B., & Ponnuswamy, V. (2022). A two-dimensional mathematical model of tumor angiogenesis with CD147. *Proceedings of the Institution of Mechanical Engineers, Part H: Journal of Engineering in Medicine*, *236*(7), 1009-1022.

Tseng, H.-c., Xiong, W., Badeti, S., Yang, Y., Ma, M., Liu, T., Ramos, C. A., Dotti, G., Fritzky, L., & Jiang, J.-g. (2020). Efficacy of anti-CD147 chimeric antigen receptors targeting hepatocellular carcinoma. *Nature communications*, *11*(1), 4810.

Voigt, H., Vetter-Kauczok, C. S., Schrama, D., Hofmann, U. B., Becker, J. C., & Houben, R. (2009). CD147 impacts angiogenesis and metastasis formation. *Cancer investigation*, *27*(3), 329-333.

Wang, B., Xu, Y.-F., He, B.-S., Pan, Y.-Q., Zhang, L.-R., Zhu, C., Qu, L.-L., & Wang, S.-K. (2010). RNAi-mediated silencing of CD147 inhibits tumor cell proliferation, invasion and increases chemosensitivity to cisplatin in SGC7901 cells in vitro. *Journal of Experimental & Clinical Cancer Research*, *29*, 1-8.

Wang, C. h., Yao, H., Chen, L. n., Jia, J. f., Wang, L., Dai, J. y., Zheng, Z. h., Chen, Z. n., & Zhu, P. (2012). CD147 induces angiogenesis through a vascular endothelial growth factor and hypoxia-inducible transcription factor 1α–mediated pathway in rheumatoid arthritis. *Arthritis & Rheumatism*, *64*(6), 1818-1827.

Wang, Y., Xie, X., Guo, X., Zhang, X., Zhang, S., Cai, J., Li, C., & Zhou, W. (2016). Research progress in CD147 as a key target of anti-angiogenic therapy in oncology. *Frontiers in Molecular Biosciences*, *3*(10), 15–25.

Weidle, U. H., Scheuer, W., Eggle, D., Klostermann, S., & Stockinger, H. (2010). Cancer-related issues of CD147. *Cancer genomics & proteomics*, *7*(3), 157-169.

Wieser, S., Weghuber, J., Sams, M., Stockinger, H., & Schütz, G. J. (2009). Cell-to-cell variability in the diffusion constants of the plasma membrane proteins CD59 and CD147. *Soft Matter*, *5*(17), 3287-3294.

Wróbel-Roztropiński, A., Zielińska-Kaźmierska, B., Roztropiński, H., Lucas-Grzelczyk, W., Szemraj, J., & Józefowicz-Korczyńska, M. (2021). Expression of matrix metalloproteinases (MMPs) and their inhibitor (TIMP) genes on mRNA and protein levels in oral squamous cell carcinoma. *Biuletyn Polskiego Towarzystwa Onkologicznego Nowotwory*, *6*(1), 1-8.

Wu, B., Wang, Y., Yang, X., Xie, B., Feng, F., Wang, B., Liang, Q., Li, Y., Zhou, Y., Jiang, J., & Chen, Z. (2013). Biallelic-intronic substitution of CD95 promotes cell signaling and tumorigenicity in hepatoblastoma carcinoma. *Journal of Experimental and Clinical Cancer Research*, *34*(9), 110–117.

Xiao, H., & Wu, R. (2017). Quantitative investigation of human cell surface N-glycoprotein dynamics. *Chemical science*, *8*(1), 268-277.

Xiong, L., Ding, L., Ning, H., Wu, C., Fu, K., Wang, Y., Zhang, Y., Liu, Y., & Zhou, L. (2016). CD147 knockdown improves the antitumor efficacy of trastuzumab in HER2-positive breast cancer cells. *Oncotarget*, *7*(36), 57737.

Yin, H., Shao, Y., & Chen, X. (2017). The effects of CD147 on the cell proliferation, apoptosis, invasion, and angiogenesis in glioma. *Neurological Sciences*, *38*, 129-136.

Zhao, G., Chen, E., Yu, X., Cui, H., Lv, J., & Wu, J. (2017). Three-dimensional model of metastatic tumor angiogenesis in response to anti-angiogenic factor angiostatin. *Journal of Mechanics in Medicine and Biology*, *17*(06), 1750094.